Production of highly polarized vapors using laser optical pumping with velocity-changing collisions

W. W. Quivers, Jr.
Department of Physics, Wellesley College, Wellesley, Massachusetts 02181
and M.I.T. Laser Research Center, Massachusetts Institute of Technology, Cambridge, Massachusetts 02131
(Received 13 December 1985; revised manuscript received 20 June 1986)

Experiments have shown the novel combination of laser optical pumping and velocity-changing collisions (between active- and buffer-gas atoms) to be very effective in producing vapors with high atomic or nuclear polarizations. This paper presents a theory which has proven successful in analyzing these experiments. The theory predicts the amount of polarization attainable for particular experimental conditions and establishes the general criteria for optimum polarization. The theory is based on sets of coupled rate equations, which contain terms describing the pumping process (i.e., stimulated absorption or emission), radiative branching, relaxation, and velocity-changing collisions. The collision terms are written in the strong-collision approximation, which assumes that a single collision, on average, thermalizes the velocity distribution. Expressions are derived for the polarization and level populations.

I. INTRODUCTION

There is considerable current interest in laser optical pumping as a technique for producing large atomic or nuclear polarization in atomic vapors.[1] Potential applications include the production of intense polarized-light ion beams by charge exchange,[2] polarized targets for nuclear physics scattering studies,[1,3–5] laser-induced nuclear orientation (LINO) (Ref. 6) studies, and for the proposed production of polarized fuels for nuclear fusion.[7]

Lasers provide intense, monochromatic collimated beams of polarized radiation, and are therefore superior to conventional optical-pumping sources. They span the spectral range from millimeter wave lengths to the uv region, and dye lasers are continuously tunable over the entire visible spectrum. Average powers of several watts are readily available. Since 1 W corresponds to a photon current of about 1 A, dense vapors can be fully polarized.

The main disadvantage of cw laser radiation is its spectral purity. When an intense monochromatic field resonantly interacts with a Doppler-broadened optical transition it selectively saturates only those atoms which are distributed over a homogeneous linewidth, ~ 10 MHz for radiative broadening. Since Doppler linewidths are $\sim 1-2$ GHz, the fraction of atoms which can be optically pumped is typically 1%. Hence the velocity selectivity of the laser, which causes poor Doppler (velocity) coverage, results in incomplete polarization.

Some current techniques designed to overcome this difficulty include the use of broadband or multimode laser radiation,[8] power broadening,[3] pressure broadening,[9,10] and buffer-gas-induced velocity-changing collisions (VCC's).[4,11] The first three methods require, respectively, stabilizing sets of randomly fluctuating modes, high laser intensities (approximately tens of W/cm^2), and high buffer-gas pressures.

Although laser optical pumping and VCC's are well known, it has only been recently demonstrated that their novel combination could produce vapors with large atomic or nuclear polarization.[4] This paper investigates single-mode laser optical pumping with VCC's as a technique for producing fully polarized vapors. This technique enables large polarizations to be produced using relatively modest laser intensities (approximately several hundred mW/cm^2). In experiments up to now the VCC's are induced by adding to the vapor small amounts of buffer-gas "perturbers" (a few tenths of a torr). In some applications this may cause unwanted background effects. However, recent laser-optical-pumping studies of low-density rubidium vapor have also shown that nondepolarizing wall-induced VCC's can also increase Doppler coverage.[12] These VCC's may eliminate the need for perturbers but are generally best suited for cases involving long relaxation times (a few milliseconds). Previously, VCC processes have been studied in both laser saturation spectroscopy[13] and in laser optical pumping.[14]

This paper presents a theory of laser optical pumping with VCC's. The results, in addition to establishing the conditions required to achieve optimum polarization, can be used to determine the amount of polarization produced in a given experiment. In order to accomplish this, the theory must adequately describe the laser optical pumping and VCC processes. The theory has been successfully applied to optical-pumping studies involving sodium,[4,11,15] lithium,[15] ytterbium,[11] and, more recently, LINO studies of the 1-μs ^{85m}Rb isomer.[16]

II. LASER OPTICAL PUMPING AND VCC's

The optical-pumping process alters the populations of the various M_F Zeeman sublevels by transferring angular momentum from the applied field to the active atoms. For example, for a right-hand circularly polarized field

resonant with an atomic transition, photons are absorbed according to the selection rule $\Delta M_F = 1$, whereas in the resulting spontaneous emission $\Delta M_F = 0$ and ± 1 transitions are all allowed. Consequently, each pumping cycle tends to shift population toward higher M_F states, resulting in ground-state orientation. Both the nucleus and atomic electrons are polarized in this process, and the sample acquires a net magnetization.

As mentioned above, in the absence of VCC's, optical pumping with a single-mode laser field polarizes only a small portion of the thermal velocity distribution. A VCC is an elastic collision which changes the velocity of an active atom without changing its orientation. Due to the spherically symmetric ground states of the active atoms and perturbers, depolarization cross sections are typically many orders of magnitude smaller than VCC cross sections.[17] Of particular interest here are strong (thermalizing) VCC's, in which the rms velocity change, Δv, is much larger than the width of the resonant velocity "bin" ($\Delta v \gg \gamma_H / k$, with γ_H the homogeneous linewidth and $k = 2\pi/\lambda$ the wave number of the transition). Strong collisions are important because they produce velocity thermalization in only a few collisions. In general, for active atom mass m_A and perturber mass m_P, strong VCC's require $m_A / mP \lesssim 1$.[18]

To ensure rapid velocity coverage the number of VCC's occurring during the ground-state orientation relaxation time T must be large compared to the total number of velocity bins,

$$\Gamma^v T \gg \frac{2ku}{\gamma_H} , \tag{1a}$$

with VCC rate Γ^v and thermal speed u (ku is the $1/e$ Doppler width). Condition (1a) assumes that there is a dominant relaxation mechanism, with characteristic time T. For the active and buffer-gas pressures of interest, the primary relaxation mechanism is cell-wall collisions. In this case T is usually the diffusion time through the cell to the walls, where depolarizing collisions occur.

The effects of VCC's on the laser-interaction process can be studied by referring to Fig. 1. The VCC's transfer pumped atoms into nonresonant velocity bins and replenish the resonant velocity bin with atoms not yet pumped. (In addition to creating velocity diffusion, the VCC's also produce spatial diffusion, which increases T.) This leads to two components in the velocity distribution, (i) a narrow feature ("dip") due to atoms that are resonant with the field and have not undergone VCC's, and (ii) a broad "pedestal" indicative of complete Doppler coverage [e.g., see Fig. 2(b)]. The relative sizes of the two features depend on the effectiveness of the VCC processes. The larger the pedestal, the more effective the VCC's. For a fixed laser intensity, the size of the pedestal increases with pressure, while that of the dip decreases. As described in detail in Sec. III, the dip can be used to obtain information about the VCC processes.

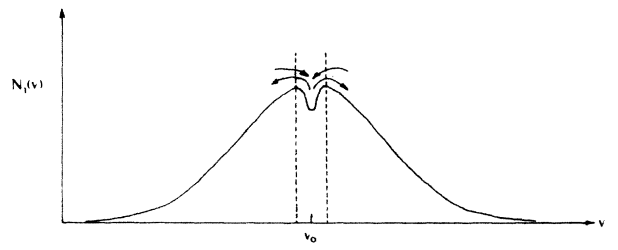

FIG. 1. Effect of VCC's on laser-optical pumping, with pump laser tuned to resonance. Buffer-gas perturbers cause VCC's into and out of the resonance velocity bin (broken vertical lines).

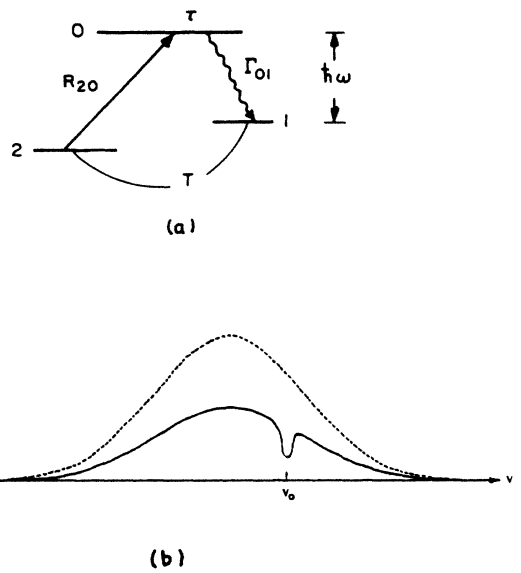

FIG. 2. (a) Optical pumping of a three-level system. R is the pumping rate, Γ_{01} and Γ_{02} are radiative-decay rates, and T is the $1 \rightarrow 2$ relaxation time. (b) Effect of VCC's and optical pumping on the velocity profile of level 2. The broken line is the zero-field equilibrium distribution of level 2, while the solid line is the optical-pumping pedestal with laser-induced narrow saturation dip centered at $V = V_0$. Here the laser is pumping the velocity line centered at $V = V_0$.

The simplest energy-level scheme for studying the optical-pumping process in atoms is the coupled three-level system shown in Fig. 2 (e.g., odd isotopes of Yb for circular-polarized radiation, see Ref. 11). It is composed of two ground-state M levels, 1 and 2, both radiatively coupled to a single excited level of energy $\hbar\omega$. Consider the system to be Doppler broadened and subjected to single-frequency pump radiation of the appropriate polarization, so that only the 2-0 transition interacts with the laser field. Atoms decay from level 0 to levels 1 and 2 with partial radiative decay rates Γ_{01} and Γ_{02}, respectively [radiative lifetime $\tau = 1/(\Gamma_{01} + \Gamma_{02})$]. Thus, atoms tend to accumulate in level 1 and are polarized. The extent of polarization is determined by the mean time T required for the excess atoms in level 1 to relax back to level 2.

Appreciable polarization requires both rapid thermalization, condition (1a), to access the entire velocity profile, and fast excited-state branching decay,

$$\Gamma_{01} T \gg 1 , \tag{1b}$$

to ensure many optical pumping cycles in a given velocity group before polarization relaxation occurs. When conditions (1a) and (1b) are satisfied the population of level 0 is negligible, and the system of Fig. 2 can be approximately described by

$$\dot{\mathcal{N}}_1=(\rho\mathscr{R})\mathcal{N}_2-\frac{(\mathcal{N}_1-\mathcal{N}_1^{(0)})}{T}\ , \tag{2a}$$

$$\mathcal{N}_1+\mathcal{N}_2=\mathcal{N}_1^{(0)}+\mathcal{N}_2^{(0)}=N_{\rm tot}\ , \tag{2b}$$

with $\mathcal{N}_1$ and $\mathcal{N}_2$ the population of levels 1 and 2, $\mathcal{N}_{1,2}^{(0)}$ are the respective thermal populations (assumed equal), and $N_{\rm tot}$ is the total atomic density. The branching ratio $\rho=\Gamma_{01}\tau$ is the probability that an atom excited from level 2 to level 0 decays to level 1, and $\mathscr{R}$ is the laser-pump rate, given by

$$\mathscr{R}=\frac{\sigma_D I}{\hbar\omega}\ , \tag{3}$$

with σ_D the 2-0 absorption cross section, and laser intensity I. The steady-state polarization is then given by

$$P=\frac{\mathcal{N}_1-\mathcal{N}_2}{\mathcal{N}_1+\mathcal{N}_2}=\frac{\rho\mathscr{R}T}{1+\rho\mathscr{R}T}\ , \tag{4a}$$

which can be rewritten in the form

$$P=\frac{I}{I+\mathscr{I}_{\rm op}}\ , \tag{4b}$$

with optical-pumping saturation intensity

$$\mathscr{I}_{\rm op}=\frac{1}{\rho}\frac{\hbar\omega}{\sigma_D}\frac{1}{T}\ . \tag{5}$$

This indicates that efficient optical pumping requires $I>\mathscr{I}_{\rm op}$, for which most of the population has been transferred to level 1 and, therefore, produces a fully polarized sample. As seen in Sec. III, Eqs. (4) follow from a more detailed theoretical model in the appropriate limit.

III. THEORY

A. General results

The basic features of the laser optical pumping process are exhibited by the three-level system of Fig. 2. The problem can be formulated in terms of coupled rate equations[19] for the population densities $N_i(\mathbf{v})$ of atoms in level i with velocities in an interval $d\mathbf{v}$ centered about $\mathbf{v}$,

$$\begin{aligned}
\dot{N}_0&=-(N_0-N_2)R_{20}-\left[\frac{1}{\tau}+\frac{1}{T}\right]N_0\\
&\quad+\left[-\Gamma_e^v N_0+\int d\mathbf{v}'W_e(\mathbf{v}'\to\mathbf{v})N_0\right]\ ,\\
\dot{N}_2&=-(N_2-N_0)R_{20}+\Gamma_{02}N_0-\left[\frac{N_2-N_2^{(0)}}{T}\right]\\
&\quad+\left[-\Gamma_g^v N_2+\int d\mathbf{v}'W_g(\mathbf{v}'\to\mathbf{v})N_2\right]\ ,\\
\dot{N}_1&=\Gamma_{01}N_0-\left[\frac{N_1-N_1^{(0)}}{T}\right]\\
&\quad+\left[-\Gamma_g^v N_1+\int d\mathbf{v}'W_g(\mathbf{v}'\to\mathbf{v})N_1\right]\ ,
\end{aligned} \tag{6}$$

with $N_i^{(0)}$ the equilibrium (thermal) populations, the terms in brackets describe the effects of VCC's, and are written in a simple "rate out minus rate in" form (see Fig. 1). The total VCC rate is given by[20]

$$\Gamma_i^v(\mathbf{v})=\int W_i(\mathbf{v}\to\mathbf{v}')d\mathbf{v}'\ , \tag{7}$$

with the collision kernel $W_i(\mathbf{v}-\mathbf{v}')$ the probability per unit time per unit velocity interval that atoms in level i experience a collision which changes their velocity from $\mathbf{v}$ to $\mathbf{v}'$. In writing the VCC terms it has been assumed that levels 1 and 2 belong to the same electronic ground state with VCC rate Γ_g^v, while level 0 is an excited electronic state with VCC rate Γ_e^v. Since the laser pumping process selects only the longitudinal component of the velocity, the problem may be treated as being one dimensional in $\mathbf{v}$, as measured along the beam axis. The laser pumping rate is given by

$$R_{20}=\frac{\sigma_{(20)H}I}{\hbar\omega}\ , \tag{8}$$

with homogeneous absorption cross section

$$\sigma_{(20)H}=\left[8\pi k\frac{|\mu_{20}|^2}{\hbar\gamma_N}\right]\frac{\gamma_N}{\gamma_H}\mathscr{L}(x)=\sigma_{(20)H}^{(0)}\mathscr{L}(x)\ , \tag{9}$$

and

$$\mathscr{L}(x)=\frac{(\gamma_H/2)^2}{(\Delta_{20}-x)^2+(\gamma_H/2)^2}\ . \tag{10}$$

The homogeneous width is $\gamma_H=1/\tau+2/T+\gamma_P$, with γ_P the contribution due to pressure broadening. The detuning of the laser frequency Ω from the atomic-center frequency ω_{20} is $\Delta_{20}=\Omega-\omega_{20}$, I is the laser intensity, $k=2\pi/\lambda$, $x=kv$ (with $v=v_z$ along the beam axis) is the Doppler frequency shift, and μ_{20} the 2-0 electric dipole matrix element.

In general, because the kernel is a function of both v and v', Eqs. (6) are quite complicated and may be solved using iterative techniques.[21] However, for strong collisions the kernel is greatly simplified and can be approximated by

$$W(v'\to v)\simeq W(v)\ , \tag{11}$$

which means that the probability that an atom has a particular velocity after a collision is unrelated to its velocity before the collision. Consequently, atoms which have undergone collisions are assumed to have a thermal distribution.

For strong collisions Eqs. (6) reduce to

$$\dot{N}_0=-(N_0-N_2)R_{20}-\left[\frac{1}{\tau}+\frac{1}{T}\right]N_0 +(-\Gamma_e^v N_0+W_e\mathcal{N}_0)\ ,$$

$$\dot{N}_2=-(N_2-N_0)R_{20}+\Gamma_{02}N_0-\left[\frac{N_2-N_2^{(0)}}{T}\right] +(-\Gamma_g^v N_2+W_g\mathcal{N}_2)\ , \tag{12}$$

$$\dot{N}_1=\Gamma_{01}N_0-\left[\frac{N_1-N_1^{(0)}}{T}\right]+(-\Gamma_g^v N_1+W_g\mathcal{N}_1)\ ,$$

where

$$\mathcal{N}_i=\int N_i(v)dv\ , \tag{13}$$

is the total population of level i. The VCC kernel is given by

$$W_{g(e)}(v)=\Gamma_{g(e)}^v G(x)\ , \tag{14}$$

with

$$G(x)=\frac{1}{ku}e^{-(x/ku)^2}\ , \tag{15}$$

the normalized $[\int G(x)dx=1]$ Gaussian distribution function.[22,23] The zero-field equilibrium populations are $N_i^{(0)}=\mathcal{N}_i^{(0)}G(x)$, with $\mathcal{N}_i^{(0)}$ the total background equilibrium density of atoms in level i. For $\mathcal{N}_1^{(0)}=\mathcal{N}_2^{(0)}$ conservation of number implies that $\mathcal{N}_1^{(0)}+\mathcal{N}_2^{(0)}=N_{\rm tot}$, the total density of atoms. Wall relaxation is included through the $(N_i-N_i^{(0)})/T$ terms.

The procedure[15] for obtaining the steady-state solutions to Eqs. (12) is straightforward. First, the equation for $\dot{N}_i=0$ must be solved for the various N_i. The resulting expressions, which are functions of both N_i and $\mathcal{N}_i$, are then integrated over velocity (x) to obtain coupled equations for he $\mathcal{N}_i$. Finally, these equations are substituted into the expressions in N_i and $\mathcal{N}_i$ found in the first step to obtain final expressions for the N_i's. All of the velocity integrations are performed in the Doppler-broadened limit $(\gamma_H, |\Delta_{20}|<|ku)$.

The first three steps of this procedure yield the following general expressions for the $\mathcal{N}_i$:

$$\mathcal{N}_0=\frac{1}{D}\frac{I}{I+I_{\rm op}}\mathcal{N}_2^{(0)}\ ,$$

$$\mathcal{N}_2=1-\frac{(1+\Gamma_{01}T)}{D}\frac{I}{I+I_{\rm op}}\mathcal{N}_2^{(0)}\ , \tag{16}$$

$$\mathcal{N}_1=1+\frac{\Gamma_{01}T}{D}\frac{I}{I+I_{\rm op}}\mathcal{N}_2^{(0)}\ ,$$

with

$$D=2+\Gamma_{01}T-\left[\frac{1}{\tau}+\frac{1}{T}\right]\left[\frac{\gamma_e+\gamma_g-\Gamma_{02}}{\gamma_e\gamma_g}\right]\ ,$$

$$\gamma_g=\Gamma_g^v+\frac{1}{T}\ , \tag{17}$$

$$\gamma_e=\frac{1}{\tau}+\Gamma_e^v+\frac{1}{T}\ .$$

The optical-pumping saturation intensity is given by

$$I_{\rm op}=\frac{1}{D}\frac{\hbar\omega}{\sigma_{(20)D}}\left[\frac{1}{\tau}+\frac{1}{T}\right]\sqrt{1+S}\ , \tag{18}$$

with Doppler-broadened absorption cross section

$$\sigma_{(20)D}=\sigma_{(20)H}^{(0)}\frac{\gamma_H\sqrt{\pi}}{2ku}e^{-(\Delta_{20}/ku)^2}\ , \tag{19}$$

and $S=I/I_S$, with the "usual" saturation intensity given by

$$I_S=\left[\frac{\gamma_e}{\gamma_e+\gamma_g-\Gamma_{02}}\right]\frac{\hbar\omega}{\sigma_{(20)H}^{(0)}}\gamma_g\ . \tag{20}$$

The last step of the procedure then gives the following general expressions for the populations:

$$N_0=\left\{\left[1-\beta_0\left[\frac{I}{I+I_{\rm op}}\right]\right]\left[\frac{\gamma_g}{\gamma_e+\gamma_g-\Gamma_{02}}\right]\frac{I}{I+I_S}L(x) +\frac{1}{D}\left[\frac{\Gamma_e^v}{\gamma_e}\right]\left[\frac{I}{I+I_{\rm op}}\right]\right\}\mathcal{N}_2^{(0)}G(x)\ ,$$

$$N_2=\left\{1-\left[1-\beta_0\left[\frac{I}{I+I_{\rm op}}\right]\right]\left[\frac{\gamma_e-\Gamma_{02}}{\gamma_e+\gamma_g-\Gamma_{02}}\right] \times\frac{I}{I+I_S}L(x)+\beta_2\left[\frac{I}{I+I_{\rm op}}\right]\right\}\mathcal{N}_2^{(0)}G(x)\ , \tag{21}$$

$$N_1=\mathcal{N}_1^{(0)}G(x)+\frac{\Gamma_{01}}{\gamma_g}\left\{\left[1-\beta_0\left[\frac{I}{I+I_{\rm op}}\right]\right] \times\left[\frac{\gamma_g}{\gamma_e+\gamma_g-\Gamma_{02}}\right]\frac{I}{I+I_S}L(x) +\beta_1\left[\frac{I}{I+I_{\rm op}}\right]\right\}\mathcal{N}_2^{(0)}G(x)\ ,$$

where

$$\beta_0=\frac{1}{\gamma_g D}\left[(1+\Gamma_{01}T)\Gamma_g^v+\left[\frac{\gamma_g-\Gamma_{02}}{\gamma_e}\right]\Gamma_e^v\right],$$
$$\beta_1=\frac{1}{D}\left[\Gamma_g^v T+\frac{\Gamma_e^v}{\gamma_e}\right], \tag{22}$$
$$\beta_2=\frac{1}{\gamma_g D}\left[\frac{\Gamma_e^v\Gamma_{02}}{\gamma_e}-(1+\Gamma_{01}T)\Gamma_g^v\right],$$

and the power-broadened Lorentzian factor

$$L(x)=\frac{(\gamma_H/2)^2(1+S)}{(\Delta_{20}-x)^2+(\gamma_H/2)^2(1+S)}. \tag{23}$$

It is convenient (but not necessary) to add a third condition,

$$\frac{1}{\tau}\gg\Gamma_e^v\gg\frac{1}{T} \tag{1'}$$

to those given earlier in Sec. II. This condition essentially decouples VCC's from radiative decay (e.g., it means that an atom pumped into the excited state decays before it experiences a velocity change).[24] This condition greatly simplifies the relevant expressions. Since many experiments of interest use only small amounts of buffer gas, condition (1') is usually satisfied. Then, employing condition (1'),

$$\begin{aligned}&D\simeq\Gamma_{01}T,\\&\beta_0\simeq 1,\\&\beta_1\simeq\Gamma_g^v/\Gamma_{01},\\&\beta_2\simeq -1,\end{aligned} \tag{24}$$

so that Eqs. (21) reduce to

$$N_0=\left[\frac{I_{\rm op}}{I+I_{\rm op}}\right]\frac{\Gamma_0^v}{\Gamma_{01}}\frac{I}{I+I_S}L(x)\mathcal{N}_2^{(0)}G(x),$$
$$N_2=\left[\frac{I_{\rm op}}{I+I_{\rm op}}\right]\left[1-\frac{I}{I+I_S}L(x)\right]\mathcal{N}_2^{(0)}G(x), \tag{25}$$
$$N_i=\mathcal{N}_1^{(0)}G(x)+\left[\frac{I}{I+I_{\rm op}}+\left[\frac{I_{\rm op}}{I+I_{\rm op}}\right]\left[\frac{I}{I+I_S}\right]L(x)\right]\times\mathcal{N}_2^{(0)}G(x).$$

Now Eqs. (16) reduce to

$$\mathcal{N}_0=\frac{1}{\Gamma_{01}T}\left[\frac{I}{I+I_{\rm op}}\right]\mathcal{N}_2^{(0)},$$
$$\mathcal{N}_2=\frac{I_{\rm op}}{I+I_{\rm op}}, \tag{26}$$
$$\mathcal{N}_1=\mathcal{N}_1^{(0)}+\frac{I}{I+I_{\rm op}}\mathcal{N}_2^{(0)},$$

where

$$I_S=\frac{1}{\rho}\frac{\hbar\omega}{\sigma_{(20)H}^{(0)}}\Gamma_g^v, \tag{27}$$

and

$$I_{\rm op}=\frac{1}{\rho}\frac{\hbar\omega}{\sigma_{(20)D}}\frac{1}{T}\sqrt{1+S}, \tag{28}$$

with $\rho=\Gamma_{01}\tau_1$ and the other quantities as defined earlier. Conditions (1) mean that $I_S\gg I_{\rm op}$, and that both $\mathcal{N}_0$ and N_0 are negligible compared to $\mathcal{N}_{1,2}$ and $N_{1,2}$.

As a laser field tuned, for example, to the 2-0 transition in Fig. 2, propagates through a sample (z direction), the change in its intensity is given by

$$\frac{dI}{dz}=\alpha I, \tag{29}$$

with velocity-integrated absorption coefficient α, which in the rate-equation approximation of Eqs. (12) is given by

$$\alpha=\int(N_0-N_2)\sigma_{(20)H}(x)dx$$
$$=-\frac{1}{\sqrt{1+S}}\mathcal{N}_2\sigma_{(20)D}. \tag{30}$$

If desired, for a sample cell of length L, Eqs. (29) and (30) can be easily manipulated to obtain $I(Z=L)$, the pump intensity at the exit face of the cell for a given intensity $I(0)$, at the input face. As discussed in Sec. III B, the results can be used to measure the sample polarization.

An interesting and perhaps unexpected result of this treatment is that $I_{\rm op}$, Eq. (28), is itself intensity dependent through the factor $\sqrt{1+S}$. This is the result of the fact that when VCC's are effective [i.e., conditions (1a) and (1b) are satisfied] the monochromatic field can saturate the entire velocity distribution. Thus, although the system behaves as a Doppler-broadened one for small intensities, it saturates as a homogeneously broadened system. Consequently, when $I\gg I_{\rm op}$ Eqs. (29) and (30) yield

$$\frac{dI}{dZ}=-\frac{1}{\rho}\frac{1}{2}N_{\rm tot}\frac{\hbar\omega}{T}, \tag{31}$$

as expected when the laser field saturates the complete velocity distribution.

The laser will essentially pump the entire Doppler distribution each optical-pumping cycle when the number of VCC's occurring per cycle is much greater than the number of pump photons. This means that when

$$\Gamma_g^v\gg R \tag{32}$$

the velocity selectivity of the single-mode laser has been effectively removed and the overall effect is the same as that for a velocity-independent broadband source. This is easily explained as follows: The laser is depleting a single velocity bin at a rate R, but since the rate Γ_g^v at which the VCC's are replenishing it with atoms from the entire Doppler distribution is so much faster, the velocity distribution remains thermalized even during the pumping process. As a result, Eqs. (6) can be directly integrated over velocity to yield the following simplified velocity-independent broadband equations:

$$\dot{\mathcal{N}}_0=-(\mathcal{N}_0-\mathcal{N}_2)\mathcal{R}_{20}-\left[\frac{1}{\tau}+\frac{1}{T}\right]\mathcal{N}_0 ,$$
$$\dot{\mathcal{N}}_2=-(\mathcal{N}_2-\mathcal{N}_0)\mathcal{R}_{20}+\Gamma_{02}\mathcal{N}_0-\left[\frac{\mathcal{N}_2-\mathcal{N}_2^{(0)}}{T}\right] , \quad (33)$$
$$\dot{\mathcal{N}}_1=\Gamma_0\mathcal{N}_0-\left[\frac{\mathcal{N}_1-\mathcal{N}_1^{(0)}}{T}\right] ,$$

with pumping rate [see Eq. (3)]

$$\mathcal{R}=\frac{\sigma_{(20)D}I}{\hbar\omega} ,$$

where $\sigma_{(20)D}$ is given by Eq. (19) and all VCC terms integrate identically to zero. The steady-state solutions are given by

$$\mathcal{N}_0=\frac{1}{\Gamma_{01}T}\left[\frac{I}{I+\mathcal{I}_{op}}\right]\mathcal{N}_2^{(0)} ,$$
$$\mathcal{N}_2=\frac{\mathcal{I}_{op}}{I+\mathcal{I}_{op}}\mathcal{N}_2^{(0)} ,$$
$$\mathcal{N}_1=\mathcal{N}_1^{(0)}+\frac{I}{I+\mathcal{I}_{op}}\mathcal{N}_2^{(0)} , \quad (34)$$

where [see Eq. (5)]

$$\mathcal{I}_{op}=\frac{1}{\rho}\frac{\hbar\omega}{\sigma_{(20)D}}\frac{1}{T} .$$

Equations (33) point out the crucial role played by VCC's in obtaining full velocity coverage in single-mode laser optical pumping. As Eqs. (8) and (27), the condition (32) show, here $I_S \gg I$ (i.e., $S \ll 1$) so that the velocity-dependent narrow-dip features discussed in Sec. II are absent [i.e., no narrow dip in Fig. 2(b)]. [Equations (33) are approximate in that they assume $S \ll 1$.]

In view of the above discussion, and for the remainder of the paper, $R \gtrsim \Gamma_g^v$ will be called the velocity-selective limit of laser optical pumping with VCC, since in this limit the velocity-dependent resonant features, such as the narrow dip in Fig. 2(b), are present. On the other hand, $\Gamma_g^v \gg R$ will be designated the broadband limit, where all velocity-dependent features have essentially vanished. It is the latter limit that is the most practical one for producing highly polarized atomic vapors, because for most cases of interest only modest laser powers (approximately a few hundred mW/cm^2) and low buffer-gas pressures (approximately a few tenths of a torr) are needed.

B. Laser-induced polarization

The quantity of central interest is the total polarization attainable for a given set of experimental conditions. As discussed in Sec. II, large polarizations require that conditions (1a) and (1b) be satisfied,

$$\Gamma_g^v T \gg \frac{2ku}{\gamma_H} , \quad (1a)$$
$$\Gamma_{01}T \gg 1 . \quad (1b)$$

The laser-induced polarization P can be conveniently defined as the normalized population difference between levels 1 and 2, averaged over the entire sample length L,

$$P=\frac{\int_0^L \mathcal{N}_1 dz-\int_0^L \mathcal{N}_2 dz}{\int_0^L \mathcal{N}_1 dz+\int_0^L \mathcal{N}_2 dz} . \quad (35)$$

Using Eqs. (26), (29), (30), and (5) this expression can be rewritten in terms of the intensity change of an incident beam of arbitrary intensity,

$$P=\frac{1}{\mathcal{N}_2^{(0)}\sigma_{(20)D}}\frac{I(0)-I(L)}{\mathcal{I}_{op}} . \quad (36)$$

Note that Eq. (36), a statement of energy balance, is valid for samples of arbitrary optical thickness (αL). For an optically thin sample ($\alpha L < 1$) It becomes Eq. (4b) of Sec. II. Hence once $\mathcal{I}_{op}$ is determined (see below), the polarization is easily found from the intensity change. Many applications of interest require highly polarized optically dense ($\alpha L \gg 1$) vapors,[1,5] and Eq. (36) is particularly useful for estimating the polarization in these cases.

C. Probe experiments

The experimental parameters I_{op} and Γ_g^v are most conveniently obtained by performing diagnostic probe field experiments on optically thin samples. The simplest such experiments are done in the Lamb-dip configuration, where a single laser field is split into counter-propagating pump and probe fields. Alternatively, a separately tunable co- or counterpropagating weak field may be used to probe the polarized vapor.

As an example, consider a diagnostic experiment using copropagating pump (frequency Ω_s) and probe (frequency Ω_p) fields resonant with the 2-0 transition of Fig. 2. Using Eq. (25) the velocity-integrated probe absorption coefficient is given by

$$\alpha_p=\int (N_0-N_2)\sigma_{(20)H}^{(0)}\mathcal{L}_p(x)dx = \left[\frac{I_{op}}{I+I_{op}}\right][1-\mathcal{M}(\Delta)]\alpha_p^{(0)} , \quad (37)$$

where $\mathcal{L}_p(x)$ is given by Eq. (10) and

$$\alpha_p^{(0)}=-\mathcal{N}_2^{(0)}\sigma_{(20)D} , \quad (38)$$

is the small signal background (i.e., $I=0$) probe-absorption coefficient. Assuming a small misalignment angle θ between pump and probe beams, $\mathcal{M}(\Delta)$ is given by

$$\mathcal{M}(\Delta)=\frac{S}{1+S}\frac{\Gamma_S}{W_S}\frac{W_S^2}{\Delta^2+W_S^2} , \quad (39)$$

where

$$\Delta=\Omega_p-\Omega_s ,$$
$$\Gamma_S=(\gamma_H/2)\sqrt{1+S} ,$$
$$W_S=(\gamma_H/2)(\sqrt{1+S}+1)+\gamma_m/2 , \quad (40)$$
$$\gamma_m=2(\theta ku)\sqrt{\ln 2} ,$$

with γ_m the broadening contribution due to the misalignment. For counterpropagating fields (including the Lamb-dip configuration) simply let $x \rightarrow -x$ in $\mathscr{L}_p(x)$ (Doppler frequency shift has opposite sign).

The desired experimental quantities are readily obtained by measuring the change in probe absorption induced, for example, by chopping the pump beam.[4] Using Eq. (37) the resulting "change signal," $\delta \equiv (\alpha_p^{(0)} L - \alpha_p L)/\alpha_p^{(0)} L$, is given by

$$\delta = \frac{I}{I+I_{\rm op}} + \frac{\Gamma_S}{W_S}\frac{S}{1+S}\frac{I_{\rm op}}{I+I_{\rm op}} L(\Delta) , \tag{41}$$

with

$$L(\Delta) = \frac{W_S^2}{\Delta^2 + W_S^2} . \tag{42}$$

The first term in Eq. (41) is the broad (Doppler width) pedestal shown in Fig. 3 and indicates velocity thermalization by VCC's of level 2, and the second term is the narrow residual-tip (resonance) feature caused by those atoms in level 2 which are in the resonant-velocity bin and, as such, have not experienced VCC's. As Fig. 3 shows, on resonance ($\Delta = 0$) the first term in Eq. (41) is the height of the pedestal-change signal at the position of the narrow dip, while the second term is the height of the dip-change signal. Thus, $I_{\rm op}$ is readily determined by measuring the size of the pedestal, and I_S, hence Γ_g^v, is found from the size of the dip. Also note that $I_{\rm op}$ is best determined at intensities where $S \ll 1$ ($I_{\rm op} \rightarrow \mathscr{I}_{\rm op}$), and only the first term is important, while I_S is most conveniently obtained when $S \gtrsim 1$, where the second term is easily measurable.

In addition to the above case where pump and probe fields interact with the same transition, it is possible to have, for example, the probe field resonant with the coupled 1-0 transition (by using opposite circular polarization). In this case the probe absorption is given by[19]

$$\alpha_p = -\left[\frac{I_{\rm op}}{I+I_{\rm op}}\right][1-\mathscr{M}(\Delta)]\alpha_p^{(0)} , \tag{43}$$

where all quantities are as defined earlier, with $\mathscr{N}_1^{(0)} = \mathscr{N}_2^{(0)}$. Since levels 1 and 2 are nearly degenerate, the change signal is given by

$$\delta = -\left[\frac{I}{I+I_{\rm op}} + \frac{\Gamma_S}{W_S}\frac{S}{1+S}\frac{I_{\rm op}}{I+I_{\rm op}} L(\Delta)\right] , \tag{44}$$

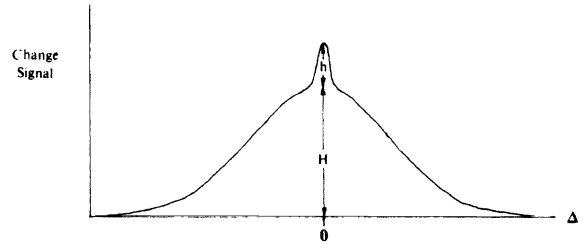

FIG. 3. Three-level change signal as a function of the pump-probe detuning $\Delta = \Omega_p - \Omega_s$. The peak heights of the pedestal and dip are denoted by H and h, respectively.

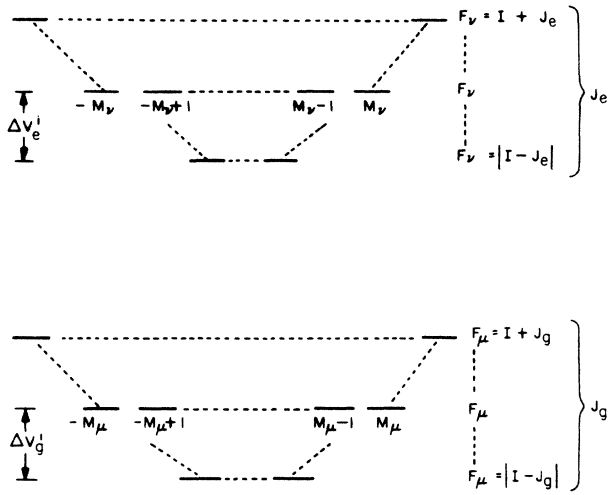

FIG. 4. General multilevel system with hf structure, where I is the nuclear spin, and $\Delta\nu_{g(e)}^i$ is the ground (excited) -state hf splitting between the ith pair of levels.

and has the same interpretation as Eq. (41). It is of opposite sign because of the increase in absorption on the 1-0 transition due to optical pumping.

IV. COMPOSITE MODEL FOR MULTILEVEL SYSTEMS

Atomic systems of interest in laser optical-pumping experiments often contain hyperfine (hf) and/or Zeeman levels and are, therefore, more complex than the ideal three-level system just discussed. In general, exact closed-form solutions are unwieldly, if at all obtainable. This section describes a model which significantly reduces the complexity of the problem.

A. The model

Consider the general multilevel system of Fig. 4, in which J_g (J_e) is the ground (excited) -state electronic angular momentum, F_μ (F_ν) is the total angular momentum (electronic plus nuclear) for a particular ground (excited) -state hf level, and the M_μ (M_ν) are the hf magnetic quantum numbers. Here the discussion will be restricted to laser optical pumping of ground S states, since only these states can undergo many VCC's before depolarization occurs, also angular momentum will be given in units of $\hbar$.

In general, a large number of coupled rate equations would be needed to describe optical pumping of a multilevel system. However, the problem can be greatly simplified by assuming that the populations of the *pumped M* states are equal throughout the pumping process. Then the pumped sublevels (here level and state will be used interchangeably) can be grouped to form either a composite level or levels (see examples below). Similarly, any *unpumped* levels in which population accumulates can also be combined into a composite level(s).

To help clarify the above points, consider the examples given in Fig. 5. For instance, Fig. 5(a) shows an

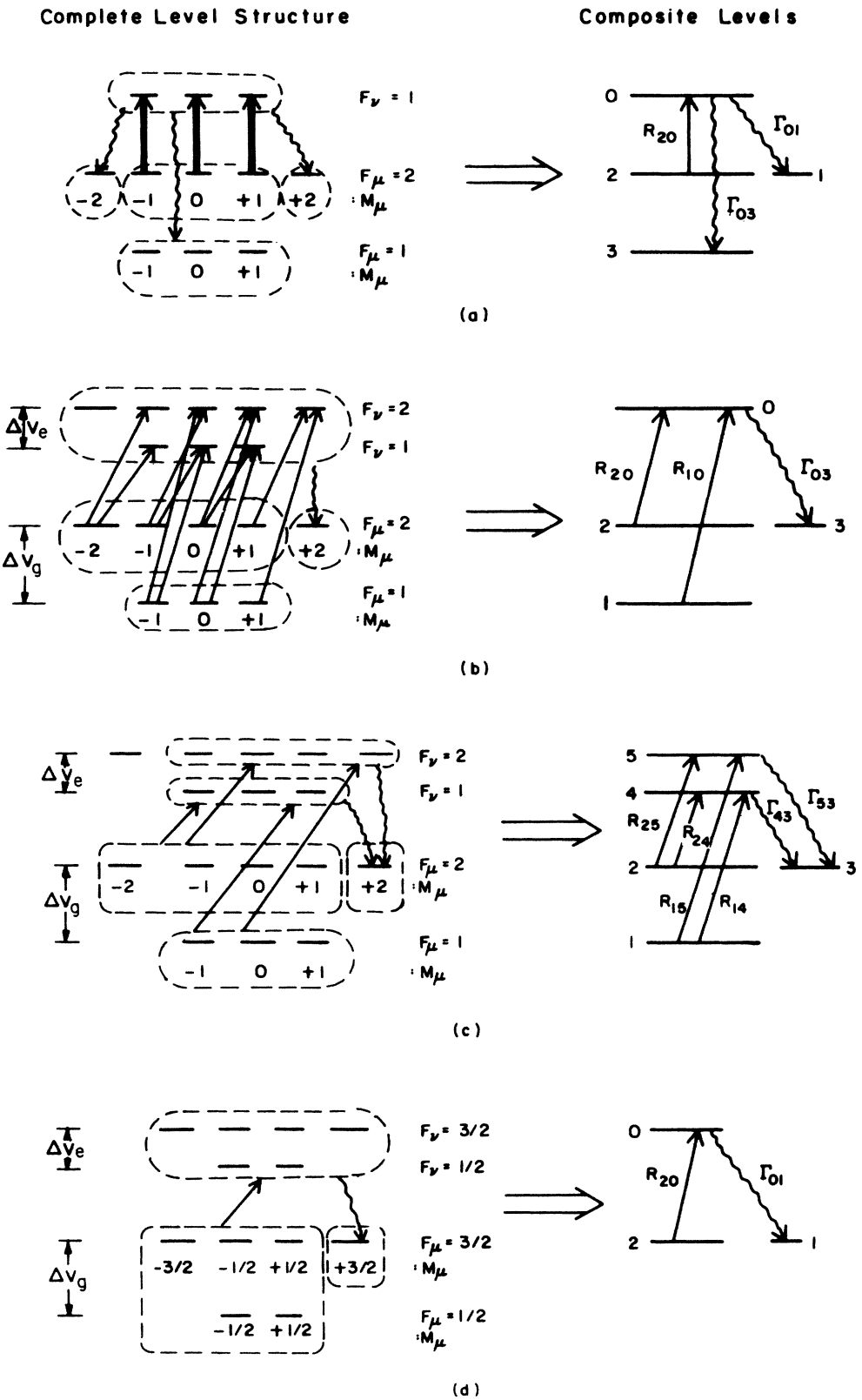

FIG. 5. (a) Linear pumping scheme. Population accumulates in the $F_\mu = 1$ level and the $M_\mu = \pm 2$ sublevels. The wavy lines indicate radiative branching to unpumped levels. (b) Pumping with circularly polarized light. Here $\Delta\nu_{g(e)}$ is the ground (excited) -state hf splitting and population is being transferred to the $M_\mu = 2$ sublevel. (c) Same as (b), but with the excited-state splitting taken into account. (d) Examples of a situation where both the excited- and ground-state hf splittings are neglected.

$F_\mu=2\rightarrow F_\nu=1$ transition being optically pumped with linearly polarized light (quantization axis parallel to direction of laser electric field). In this example, the pumped ground-state sublevels $M_\mu=0$ and ±1 of the $F_\mu=2$ level are assumed equal and grouped together to form composite level 2, the two unpumped ground-state sublevels $M_\mu=\pm2$ form composite level 1, the three unpumped $F_\mu=1$ sublevels constitute level 3, and, finally, the three excited-state sublevels of the $F_\nu=1$ level form the third composite level 0. Groupings for some other cases of interest are shown in Figs. 5(b)–5(d).

Now consider in more detail a single ground-state hf level of an optically pumped atom that has degenerate hf sublevels, i.e., degenerate M_μ's. The model assumes that all the sublevels within a particular group have equal populations. This means that, if all hf sublevels are pumped they are assumed to have equal populations and all are included in the group, which is then treated as a pumped composite level [as is the $F_\mu=1$ level in Fig. 5(b)]. Likewise, if none of the hf sublevels are pumped they also are assumed to have equal populations and are grouped together to form an unpumped composite level [$F_\mu=1$ level in Fig. 5(a)]. For hf levels in which only some of the sublevels are pumped, the populations of the pumped and unpumped sublevels are separately assumed equal and are grouped into pumped and unpumped composite levels [as with the $F_\mu=2$ level of Fig. 5(a)]. The total population of each composite level can then be defined as

$$N_\mu=\sum_{M_\mu} n_\mu(M_\mu)\equiv g_\mu n_\mu \tag{45}$$

where n_μ is the population of each sublevel in the group (composite level), with all sublevel populations assumed equal, and g_μ is the corresponding number of sublevels. Note that when all sublevels are either pumped or unpumped $g_\mu=2F_\mu+1$ [e.g., in Fig. 5(b) $g_\mu=3$ for the $F_\mu=1$ level]. The overall polarization or orientation depends on the population of the unpumped ground-state hf level(s) or sublevel(s).

Consider now the excited state of the optically pumped atom. In most cases of interest the populations of the excited hf sublevels remain negligible during the pumping process, due to fast radiative decay. So for the remainder of the paper very small excited-state populations will be assumed. Since any unpumped excited-state sublevels do not contribute in any way to the pumping process, they can be ignored. Then the population for each pumped excited-state composite level is given by

$$N_\nu=\sum_{M_\nu} n_\nu(M_\nu)\equiv g_\nu n_\nu \ , \tag{46}$$

where g_ν is the number of *pumped* sublevels in the excited-state hf level F_ν of interest, and n_ν is the corresponding sublevel population. For example, only the four pumped sublevels of the $F_\nu=2$ level in Fig. 5(c) are considered and treated equally, so $g_\nu=4$.

Now before any approximation is made (plus making a small change in notation, discussed below), consider the rate equation for a particular ground (lower 1) state sublevel, $n_l=n_l(M_\mu)$, given by

$$\dot{n}_l=-\sum_u(n_l-n_u)r_{lu}+\sum_u\gamma_{ul}n_u-\frac{(n_l-n_l^{(0)})}{T}+\left[-\Gamma_g^v n_l+W_g\int n_l dv\right] , \tag{47}$$

where $n_u=n_u(M_\nu)$ is the population of a single excited (upper u) state sublevel. The first term is the laser-pumping contribution, with the sum covering only those excited-state sublevels interacting via the laser field with n_l. The second term is the radiative-decay contribution, where the sum takes into account the branching over all excited sublevels of interest. The remaining terms describe the effects of wall collisions and VCC's.

The specific form of the quantities appearing in Eq. (47) are generalizations of Eqs. (12) of Sec. III. The laser-pumping rate per atom is given by

$$r_{ul}=\frac{\sigma_{ul}I}{\hbar\omega}\mathscr{L}_{lu}(x) \ , \tag{48}$$

where the Lorentzian line-shape factor is now

$$\mathscr{L}_{lu}(x)=\frac{(\gamma_H/2)^2}{(\Delta_{lu}-x)^2+(\gamma_H/2)^2} \ , \tag{49}$$

with $\Delta_{lu}=\Omega-\omega_{lu}$ the detuning of the laser field, frequency Ω, from the transition frequency ω_{lu}. The homogeneous absorption cross section for the $l\rightarrow u$ transition is given by

$$\sigma_{lu}=\frac{8\pi k}{\hbar\gamma_N}|\boldsymbol{\mu}_{lu}\cdot\hat{\boldsymbol{\epsilon}}|^2=(3\beta_{lu})6\pi\lambda\!\!\!^{-2}\frac{\gamma_N}{\gamma_H} \ , \tag{50}$$

where $\gamma_N=1/\tau$, and γ_H is the homogeneous width. Here β_{lu} is defined as

$$\beta_{lu}\equiv\frac{|\boldsymbol{\mu}_{lu}\cdot\hat{\boldsymbol{\epsilon}}|^2}{\mu_0^2} \ , \tag{51}$$

with μ_0 the reduced radial dipole moment, μ_{lu} is the optical electric dipole moment, and $\hat{\epsilon}$ is the unit vector describing the polarization state of the laser field (circular or linear). The $6\pi\lambda\!\!\!^{-2}$ factor ($\lambda\!\!\!^{-}=\lambda/2\pi$) is the total absorption cross section ($S\rightarrow P$ transitions) for light of a definite polarization, and the extra factor of 3 covers the three possible polarizations. The spontaneous decay rate is given by

$$\gamma_{ul}=\frac{4}{3}\frac{k^3}{\hbar}|\boldsymbol{\mu}_{ul}|^2=\beta_{ul}\frac{3}{\tau} \ . \tag{52}$$

Note that the first sum in Eq. (47) is only over those upper-state sublevels directly coupled by the polarization selection rule of the laser field. On the other hand, because of spontaneous-decay 'selection rules, the second sum can contain levels connected by all possible polarizations.

The composite rate equation for a particular collection

of pumped ground-state sublevels is found by summing Eq. (47) over those sublevels. (For unpumped sublevels $r_{lu}=0$.) Then the rate equation for a pumped composite level is given by

$$\dot{N}_l=-\sum_l\sum_u\left[\frac{N_l}{g_l}-\frac{N_u}{g_u}\right]r_{lu}+\sum_l\sum_u\gamma_{ul}\frac{N_u}{g_u}-\frac{(N_l-N_l^{(0)})}{T}+(-\Gamma_g^v N_l+W_g\mathcal{N}_l)\ , \tag{53}$$

where definitions (45) and (46) have been used to write

$$\sum_l n_l=N_l=g_l n_l\ ,$$
$$\sum_u n_u=N_u=g_u n_u\ , \tag{54}$$
$$\int\sum_l n_l dv=\mathcal{N}_l\ ,$$

with $g_l(g_u)$ the degeneracy of the lower (upper) composite levels.

Equation (53) can be rewritten more compactly in terms of a *total* optical pumping rate R_{ul} and an *average* spontaneous decay rate Γ_{ul},

$$\dot{N}_l=-\left[\frac{N_l}{g_l}-\frac{N_u}{g_u}\right]R_{lu}+\Gamma_{ul}N_u-\frac{(N_l-N_l^{(0)})}{T}+(-\Gamma_g^v N_l+W_g\mathcal{N}_l)\ . \tag{55}$$

Here the total pumping rate is the sum of the individual pumping rates r_{lu} [see Eq. (48)] over all pairs of pumped ground and excited-state sublevels and is given by

$$R_{lu}=\sum_l\sum_u r_{lu}=\frac{\sigma_{(lu)H}^{\rm tot}I}{\hbar\omega}\mathscr{L}_{lu}(x)\ , \tag{56}$$

where $\sigma_{(lu)H}^{\rm tot}$ is the total homogeneous absorption cross section

$$\sigma_{(lu)H}^{\rm tot}=\sum_l\sum_u\sigma_{lu}=(3\beta)6\pi\lambda\!\!\!^{-2}\frac{\gamma_N}{\gamma_H}\ , \tag{57}$$

with $\beta\equiv\sum_l\sum_u\beta_{lu}$. The average excited-state decay rate is defined as the sum of the individual spontaneous rates [see Eq. (52)] contributing to the decay divided by the number of participating excited-state sublevels, and is given by

$$\Gamma_{ul}=\frac{1}{g_u}\sum_l\sum_u\gamma_{ul}=\eta\frac{1}{\tau}\ , \tag{58}$$

where $\eta=(3/g_u)\sum_l\sum_u\beta_{ul}$. (Keep in mind that β and η are subject to the laser polarization and spontaneous-decay selection rules, respectively.)

Similarly, the rate equation for a single excited-state sublevel $n_u(M_v)$ can be written as

$$\dot{n}_u=-\sum_l(n_u-n_l)r_{ul}-\left[\frac{1}{\tau}+\frac{1}{T}\right]n_u+\left[-\Gamma_e^v n_u+W_e\int n_u dv\right]\ , \tag{59}$$

with terms as defined earlier, and $r_{ul}=r_{lu}$. The composite excited-state rate equation is given by

$$\dot{N}_u=-\left[\frac{N_u}{g_u}-\frac{N_l}{g_l}\right]R_{ul}-\left[\frac{1}{\tau}+\frac{1}{T}\right]N_u+\left[\Gamma_e^v N_u+W_e\mathcal{N}_u\right]\ . \tag{60}$$

As will be seen below Eqs. (55) and (60) can describe both single as well as groups of hf levels, hence the more general notation of l and u.

Equations (55) and (60) enable models containing many coupled rate equations (used in describing complicated multilevel atomic systems) to be replaced by much simpler composite models, such as the three- and four-level ones discussed in Sec. IV B below. Note that, the most convenient form for the composite rate equations is that of average populations multiplying total pumping rates and total populations multiplying average spontaneous decay rates. This is because, in some cases (see below), the equations can be written down by inspection.

It is possible to simplify the composite rate equations when the excited-state hf splitting is experimentally unresolvable.[25] If, in addition, the pump field connects each ground-state hf level to all excited-state hf levels, the excited hf splitting can be neglected. In this case all excited-state hf levels can be grouped into a single excited-state composite level [e.g., see Fig. 5(b)]. Then the sum rules cause Eqs. (57) and (58) to simplify to

$$\sigma_{(lu)H}^{\rm tot}=\bar{g}_l 2\pi\lambda\!\!\!^{-2}\frac{\gamma_N}{\gamma_H}\ , \tag{61}$$

$$\Gamma_{ul}=\frac{g_l}{g_u^{\rm tot}}\frac{1}{\tau}\ , \tag{62}$$

where $g_u^{\rm tot}=\sum_v(2F_v+1)$ is the *total* number of excited-state sublevels (*including* any unpumped ones), and $\bar{g}_l=(2F_\mu+1)$. Note that here *every* sublevel (including those not pumped) of the ground-state hf level contribute to $\sigma_{(lu)H}^{\rm tot}$. For example, four of the five sublevels in the $F_\mu=2$ level in Fig. 5(b) are pumped giving $g_l=4$ and $\bar{g}_l=5$, whereas for the excited state $g_u^{\rm tot}=8$, so $\Gamma_{02}=\frac{1}{2}(1/\tau)$ and $\sigma_{(20)H}^{\rm tot}=10\pi\lambda\!\!\!^{-2}(\gamma_N/\gamma_H)$. These results are entirely due to the properties of the matrix elements.

Equations (61) and (62) can also be used when *both* the excited and ground-state hf splittings are experimentally unresolvable.[26] In this case all ground-state levels can be treated as degenerate, and, then, pumped and unpumped sublevels can be separately combined into single pumped and unpumped composite levels for each group. Here *every* ground-state sublevel contributes to Eq. (61), so $\bar{g}_l\rightarrow g_l^{\rm tot}=\sum_u(2F_\mu+1)$, while g_l is unchanged in Eq. (62) [e.g., in Fig. 5(d) $\bar{g}_l=6$ but $g_l=1$ and 5, and $g_u^{\rm tot}=6$].

It is important to remember that Eqs. (61) and (62) can only be used for those transitions in which all excited-state hf levels are accessible to all ground-state hf levels (i.e., when $\Delta F=0$ or ±1). This condition is violated, for example, for alkali $D2$ transitions where $\Delta F=2$ would also be required. Equations (61) and (62) are useful be-

cause they are independent of the matrix elements, in contrast to Eqs. (57) and (58), and so enable the composite rate equations to be written down by inspection. These points are further discussed in Sec. IV B. Also, as some of the examples in Sec. IV B will demonstrate, the model can also be applied to atomic systems which are pumped by more than a single laser transition.

The composite model can also be applied to the broadband limit (see Sec. III), where highly polarized vapors are most conveniently produced. Velocity integration of Eqs. (55) and (60) give

$$\dot{\mathcal{N}}_l = -\left[\frac{\mathcal{N}_l}{g_l}-\frac{\mathcal{N}_u}{g_u}\right]\mathcal{R}_{lu}+\Gamma_{ul}\mathcal{N}_u-\frac{(\mathcal{N}_l-\mathcal{N}_l^{(0)})}{T}\,, \tag{63}$$

$$\dot{\mathcal{N}}_u = -\left[\frac{\mathcal{N}_u}{g_u}-\frac{\mathcal{N}_l}{g_l}\right]\mathcal{R}_{lu}-\left[\frac{1}{\tau}+\frac{1}{T}\right]\mathcal{N}_u\,. \tag{64}$$

The total broadband pumping rate is given by

$$\mathcal{R}_{lu}=\frac{\sigma^{\rm tot}_{(lu)D}I}{\hbar\omega}\,, \tag{65}$$

where $\sigma^{\rm tot}_{(lu)D}$ is the total Doppler-broadened absorption cross section

$$\sigma^{\rm tot}_{(lu)D}=\sigma^{\rm tot}_{(lu)H}\frac{\gamma_H\sqrt{\pi}}{2ku}e^{-(\Delta/ku)^2}\,, \tag{66}$$

with $\sigma^{\rm tot}_{(lu)H}$ and Γ_{ul} given by Eqs. (57) and (58), respectively, and ku is the $1/e$ Doppler width.

B. Examples

In this section some specific examples which employ the composite model are presented. They have been used in Refs. 4, 11, and 15. In the experiments only a single pump laser was used. The more complicated case involving two or more independently tunable lasers (e.g., see Ref. 16) is treated in Appendix A.

1. ^6Li

Consider laser optical pumping of the ^{6}Li-$D1$ transition which lies at $\lambda=670.8$ nm, with $\tau=27$ nsec. In fact, Fig. 5(d) shows this transition pumped by circularly polarized light. The electronic and nuclear spins are $J_g(J_e)=\frac{1}{2}$ and $I=1$, respectively, giving total atomic angular momentum $F_\mu(F_\nu)=\frac{1}{2},\frac{3}{2}$. The transition consists of two hf levels in both the ground and excited states for a total of 12 Zeeman sublevels (six in each state). The ground ($\Delta\nu_g$) and excited -state ($\Delta\nu_e$) hf splittings of 228 and 26 MHz, respectively, are much smaller than the usual Doppler width of about 4 GHz (temperatures $\sim$400–500 °C). Then, providing that they are experimentally unresolved, both the ground (excluding unpumped sublevels) and excited -state hf levels can be combined into single ground and excited pumped (including any excited unpumped sublevels) composite levels (see Sec. IV A), as depicted in Fig. 5(d). Thus, the 12-level system is replaced by the much simpler composite three-level one in the figure. The six excited-state sublevels form level 0, the five pumped ground-state sublevels form level 2, and the single unpumped ground-state sublevel [$M_\mu=\frac{3}{2}$ ($-\frac{3}{2}$) for right (left) circular polarizations] is level 1. Using Eqs. (55) and (60), the rate equations describing the composite three-level system in the velocity-selective limit are given by

$$\begin{aligned}
\dot{N}_0 &= -\left[\frac{N_0}{6}-\frac{N_2}{5}\right]R_{20}-\left[\frac{1}{\tau}+\frac{1}{T}\right]N_0 \\
&\quad +(-\Gamma_e^v N_0+W_e\mathcal{N}_0)\,, \\
\dot{N}_2 &= -\left[\frac{N_2}{5}-\frac{N_0}{6}\right]R_{20}+\Gamma_{02}N_0-\frac{(N_2-N_2^{(0)})}{T} \\
&\quad +(-\Gamma_g^v N_2+W_g\mathcal{N}_2)\,, \\
\dot{N}_1 &= \Gamma_{01}N_0-\frac{(N_1-N_1^{(0)})}{T}+(-\Gamma_g^v N_1+W_g\mathcal{N}_1)\,,
\end{aligned} \tag{67}$$

where $g_u^{\rm tot}=g_l^{\rm tot}=6$, $g_1=1$ $g_2=5$, $N_{1,2}^{(0)}=(\frac{1}{6},\frac{5}{6})N_{\rm tot}G(x)$, with $N_{\rm tot}$ the total density of atoms, and $G(x)$ is given by Eq. (15). The total laser-pumping rate is given by

$$R_{20}=\frac{\sigma^{\rm tot}_{(20)H}I}{\hbar\omega}\mathcal{L}_{20}(x)\,, \tag{68}$$

where

$$\sigma^{\rm tot}_{(20)H}=g_l^{\rm tot}2\pi\lambda^2\frac{\gamma_N}{\gamma_H}=12\pi\lambda^2\frac{\gamma_N}{\gamma_H}\,, \tag{69}$$

with the Lorentzian factor

$$\mathcal{L}_{20}(x)=\frac{(\gamma_H/2)^2}{(\Delta_{20}-x)^2+(\gamma_H/2)^2}\,, \tag{70}$$

where $x=kv$, and $\Delta_{20}=\Omega-\omega_{20}$ is the detuning, the laser frequency Ω from the transition frequency ω_{20}. The average decay rates are given by

$$\begin{aligned}
\Gamma_{01} &= \frac{g_1}{g_u^{\rm tot}}\frac{1}{\tau}=\frac{1}{6}\frac{1}{\tau}\,, \\
\Gamma_{02} &= \frac{g_2}{g_u^{\rm tot}}\frac{1}{\tau}=\frac{5}{6}\frac{1}{\tau}\,.
\end{aligned} \tag{71}$$

Note that as it should, $\Gamma_{01}+\Gamma_{02}=1/\tau$, and as expected Eqs. (67) are of the same form as Eqs. (12) for the actual three-level case, but with average populations, total rates, etc. The composite three-level system is compared to the complete 12-level one in Appendix B.

2. ^{23}Na

As another example, consider laser optical pumping of the ^{23}Na-$D1$ transition with circularly polarized radiation. The transition lies at $\lambda=589.6$ nm, with $\tau=16$ nsec. Here $J_g(J_e)=\frac{1}{2}$, $I=\frac{3}{2}$, $F_\mu(F_\nu)=1,2$, so, for example, as shown in Figs. 5(b) and 5(c), the transition contains two ground and two excited -state hf levels, for a total of sixteen hf Zeeman sublevels. The excited-state hf splitting of

189 MHz is much smaller than the 1772-MHz splitting of the ground state. Consider for the moment experiments performed in the broadband limit (see Sec. III), where the excited-state hf splitting is completely unresolved. However, the ground-state splitting is partially resolved since it is comparable to the Doppler width (~ 2 GHz, for $T \sim 120$ °C). Therefore, to a first approximation, the 16-level system of Fig. 5(b) can be replaced by the accompanying composite four-level one with effective pumping and spontaneous-decay rates. In the figure, the four pumped sublevels belonging to the $F_\mu = 2$ ground-state level and the three pumped sublevels of the $F_\mu = 1$ level form levels 2 and 1, respectively, the eight excited-state sublevels comprise level 0 and, finally, the single, unpumped ground-state sublevel [$M_\mu = 2$ (-2) for right (left) circularly polarized light] is level 3 (population accumulates in this sublevel).

The rate equations are given by

$$\begin{aligned}
\dot{\mathcal{N}}_0 &= -\left[\frac{\mathcal{N}_0}{8} - \frac{\mathcal{N}_1}{3}\right]\mathcal{R}_{10} - \left[\frac{\mathcal{N}_0}{8} - \frac{\mathcal{N}_2}{4}\right]\mathcal{R}_{20} \\
&\quad - \left[\frac{1}{\tau} + \frac{1}{T}\right]\mathcal{N}_0 , \\
\dot{\mathcal{N}}_1 &= -\left[\frac{\mathcal{N}_1}{3} - \frac{\mathcal{N}_0}{8}\right]\mathcal{R}_{10} + \Gamma_{01}\mathcal{N}_0 - \left[\frac{\mathcal{N}_1 - \mathcal{N}_1^{(0)}}{T}\right] , \\
\dot{\mathcal{N}}_2 &= -\left[\frac{\mathcal{N}_2}{4} - \frac{\mathcal{N}_0}{8}\right]\mathcal{R}_{20} + \Gamma_{02}\mathcal{N}_0 - \left[\frac{\mathcal{N}_2 - \mathcal{N}_2^{(0)}}{T}\right] , \\
\dot{\mathcal{N}}_3 &= \Gamma_{03}\mathcal{N}_0 - \left[\frac{\mathcal{N}_3 - \mathcal{N}_3^{(0)}}{T}\right] ,
\end{aligned} \tag{72}$$

where $g_u^{\text{tot}} = 8$, $g_1(\text{level } 1) = 3$, $g_2(\text{level } 2) = 4$, $g_3(\text{level } 3) = 1$, and $\mathcal{N}_{1,2,3}^{(0)} = (\frac{3}{8}, \frac{1}{2}, \frac{1}{8})N_{\text{tot}}$. Because of the large ground-state hf splitting there are two laser transitions with pumping rates given by

$$\begin{aligned}
\mathcal{R}_{10} &= \frac{\sigma_{(10)D}^{\text{tot}} I}{\hbar\omega} , \\
\mathcal{R}_{20} &= \frac{\sigma_{(20)D}^{\text{tot}} I}{\hbar\omega} ,
\end{aligned} \tag{73}$$

where, using Eqs. (61) and (66)

$$\begin{aligned}
\sigma_{(10)D}^{\text{tot}} &= 6\pi\lambda^2 \frac{\gamma_H \sqrt{\pi}}{2ku} e^{-(\Delta_{10}/ku)^2} , \\
\sigma_{(20)D}^{\text{tot}} &= 10\pi\lambda^2 \frac{\gamma_H \sqrt{\pi}}{2ku} e^{-(\Delta_{20}/ku)^2} ,
\end{aligned} \tag{74}$$

and

$$\Delta_{10}(\Delta_{20}) = \Omega - \omega_{10}(\omega_{20}) . \tag{75}$$

The average decay rates [see Eq. (62)] are given by

$$\begin{aligned}
\Gamma_{01} &= \frac{3}{8}\frac{1}{\tau} , \\
\Gamma_{02} &= \frac{1}{2}\frac{1}{\tau} , \\
\Gamma_{03} &= \frac{1}{8}\frac{1}{\tau} ,
\end{aligned} \tag{76}$$

with $\Gamma_{01} + \Gamma_{02} + \Gamma_{03} = 1/\tau$.

Now consider velocity-selective ^{23}Na experiments, where the excited-state hf splitting is resolved. This splitting results in nine experimentally observed narrow resonance features (actually there are 16 but nine are degenerate).[15] In this case, as was done for the ground state, the excited-state hf levels must be considered separately. This leads to the five-level system shown in Fig. 5(c). Here level 4 contains the three excited sublevels for $F_\nu = 1$ and level 5 the four pumped sublevels for $F_\nu = 2$, the other levels remain as before. Here equations (57) and (58) must be used in determining the composite rate equations for the five-level system. The matrix elements are given in Fig. 6, where the fractions are just the β's. Then the rate equations are given by

$$\begin{aligned}
\dot{N}_5 &= -\left[\frac{N_5}{4} - \frac{N_1}{3}\right]R_{15} - \left[\frac{N_5}{4} - \frac{N_2}{4}\right]R_{25} - \left[\frac{1}{\tau} + \frac{1}{T}\right]N_5 + (-\Gamma_e^v N_5 + W_e \mathcal{N}_5) , \\
\dot{N}_4 &= -\left[\frac{N_4}{3} - \frac{N_1}{3}\right]R_{14} - \left[\frac{N_4}{3} - \frac{N_2}{4}\right]R_{24} - \left[\frac{1}{\tau} + \frac{1}{T}\right]N_4 + (-\Gamma_e^v N_4 + W_e \mathcal{N}_4) , \\
\dot{N}_2 &= -\left[\frac{N_2}{4} - \frac{N_4}{3}\right]R_{24} - \left[\frac{N_2}{4} - \frac{N_5}{4}\right]R_{25} + \Gamma_{42}N_4 + \Gamma_{52}N_4 - \left[\frac{N_2 - N_2^{(0)}}{T}\right] + (-\Gamma_g^v N_2 + W_g \mathcal{N}_2) , \\
\dot{N}_1 &= -\left[\frac{N_1}{3} - \frac{N_4}{3}\right]R_{14} - \left[\frac{N_1}{3} - \frac{N_5}{4}\right]R_{15} + \Gamma_{41}N_4 + \Gamma_{51}N_1 - \left[\frac{N_1 - N_1^{(0)}}{T}\right] + (-\Gamma_g^v N_1 + W_g \mathcal{N}_1) , \\
\dot{N}_3 &= \Gamma_{43}N_4 + \Gamma_{53}N_3 - \left[\frac{N_3 - N_3^{(0)}}{T}\right] + (-\Gamma_g^v N_3 + W_g \mathcal{N}_3) ,
\end{aligned} \tag{77}$$

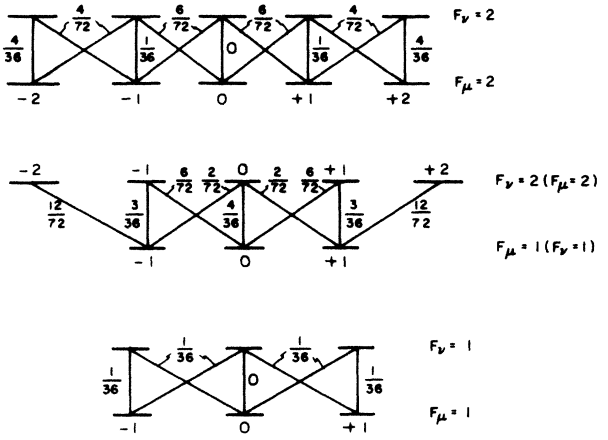

FIG. 6. ^{23}Na-$D1$ matrix elements. The numbers are the β's defined by Eq. (51).

where $g_4(\text{level } 4)=3$, $g_5(\text{level } 5)=4$, $g_1(\text{level } 1)=3$, $g_2(\text{level } 2)=4$, $g_3(\text{level } 3)=1$, and $N^{(0)}_{1,2,3}=\mathcal{N}^{(0)}_{1,2,3}G(x)$. The pumping rates for the four laser transitions are given by

$$R_{lu}=\frac{\sigma^{\text{tot}}_{(lu)}I}{\hbar\omega}\mathscr{L}_{lu}(x)\ , \tag{78}$$

where $l(u)=1,2$ (4,5) and

$$\left.\begin{aligned}\sigma^{\text{tot}}_{(14)H}&=\tfrac{1}{3}\\ \sigma^{\text{tot}}_{(15)H}&=\tfrac{5}{3}\\ \sigma^{\text{tot}}_{(24)H}&=\tfrac{5}{4}\\ \sigma^{\text{tot}}_{(25)H}&=\tfrac{5}{4}\end{aligned}\right\}\times\pi\lambda\!\!\!^{-2}\frac{\gamma_N}{\gamma_H} \tag{79}$$

and the average spontaneous-decay rates are given by

$$\begin{aligned}\Gamma_{41}&=\frac{1}{6}\frac{1}{\tau},\quad \Gamma_{51}=\frac{1}{2}\frac{1}{\tau}\ ,\\ \Gamma_{42}&=\frac{2}{3}\frac{1}{\tau},\quad \Gamma_{52}=\frac{3}{8}\frac{1}{\tau}\ ,\\ \Gamma_{43}&=\frac{1}{6}\frac{1}{\tau},\quad \Gamma_{53}=\frac{1}{8}\frac{1}{\tau}\ .\end{aligned} \tag{80}$$

The general procedure for solving the composite rate equations in the steady state is presented in Appendix A. However, as an example, the solutions to Eqs. (72) are given below,

$$\begin{aligned}\frac{\mathcal{N}_0}{N_{\text{tot}}}&=\left[\frac{\tau}{T}\right]\frac{(3/5)\mathscr{L}_1+\mathscr{L}_2}{1+\mathscr{L}_1+\mathscr{L}_2+\frac{2}{5}\mathscr{L}_1\mathscr{L}_2}\ ,\\ \frac{\mathcal{N}_1}{N_{\text{tot}}}&=\frac{(3/4)\mathscr{L}_2+3/8}{1+\mathscr{L}_1+\mathscr{L}_2+(2/5)\mathscr{L}_1\mathscr{L}_2}\ ,\\ \frac{\mathcal{N}_2}{N_{\text{tot}}}&=\frac{(4/5)\mathscr{L}_1+1/2}{1+\mathscr{L}_1+\mathscr{L}_2+(2/5)\mathscr{L}_1\mathscr{L}_2}\ ,\\ \frac{\mathcal{N}_3}{N_{\text{tot}}}&=(\Gamma_3\tau)\frac{(3/5)\mathscr{L}_1+\mathscr{L}_2}{1+\mathscr{L}_1+\mathscr{L}_2+(2/5)\mathscr{L}_1\mathscr{L}_2}+\frac{1}{8}\ ,\end{aligned} \tag{81}$$

where $\mathscr{L}_i=I/\mathscr{I}^{(i)}_{\text{op}}$ with

$$\begin{aligned}\mathscr{I}^{(1)}_{\text{op}}&=\frac{1}{\rho_1}\frac{\hbar\omega}{\bar{\sigma}_{(10)D}}\frac{1}{T}\ ,\\ \mathscr{I}^{(2)}_{\text{op}}&=\frac{1}{\rho_2}\frac{\hbar\omega}{\bar{\sigma}_{(20)D}}\frac{1}{T}\ .\end{aligned} \tag{82}$$

The branching ratios and average cross section [see Eq. (A5)] are given by

$$\begin{aligned}\rho_1&=(\Gamma_{02}+\Gamma_{03})\tau=\tfrac{5}{8}\ ,\\ \rho_2&=(\Gamma_{01}+\Gamma_{03})\tau=\tfrac{1}{2}\ ,\end{aligned} \tag{83}$$

and

$$\begin{aligned}\bar{\sigma}_{(10)D}&=2\pi\lambda\!\!\!^{-2}\frac{\gamma_H\sqrt{\pi}}{2ku}e^{-(\Delta_{10}/ku)^2}\ ,\\ \bar{\sigma}_{(20)D}&=\tfrac{5}{4}\pi\lambda\!\!\!^{-2}\frac{\gamma_H\sqrt{\pi}}{2ku}e^{-(\Delta_{20}/ku)^2}\ .\end{aligned} \tag{84}$$

It is important to keep in mind that the sodium four- and five-level models only refer to different *experimental* situations. In the first case, the excited-state hf splitting is not resolvable, whereas in the second it is.

When population accumulates in an unpumped ground-state hf level(s) hyperfine or F-optical pumping is taking place. Otherwise, when population accumulates in an unpumped sublevel(s) M_F pumping occurs. In general, I_{op} is significantly larger for the latter case.

V. SUMMARY AND DISCUSSION

As noted elsewhere (e.g., see Refs. 4 and 11) laser optical pumping with VCC is very effective in producing highly polarized atomic vapors. The theory presented in this paper uses coupled rate equations[19] to model the optical-pumping process. The equations contain laser pumping (i.e., stimulated absorption or emission), radiative decay, relaxation (e.g., diffusion to the cell walls), and VCC terms. The collision terms are written in the strong- (large-angle) collision approximation, where typical VCC cross sections are a few tens of Å^2. The theory not only predicts the amount of polarization attainable in a given experiment but also establishes the criteria that must be met in order to achieve optimum polarization. Several experiments[4,11,16] have demonstrated the theory's feasibility.

The treatment of multilevel systems presented in Sec. IV can also be applied to the no-VCC limit, where the collision terms are absent from Eqs. (55) and (60). A comparison of the numerical result for a 40-level system (corresponding to the $D1$ transition in ^{85m}Rb) (Ref. 16) was made with that of an analytically solved five-level model, and reasonable agreement between the two ($<15\%$) was found.[27]

ACKNOWLEDGMENT

The author is very grateful to Professor Michael S. Feld for many stimulating discussions and for his enthusiastic support and encouragement in this work. This work was performed at the MIT Laser Research Center, which is a

National Science Foundation Regional Instrumentation Facility.

APPENDIX A: STEADY-STATE SOLUTIONS FOR MULTILEVEL SYSTEMS

In this appendix some general procedures for solving multilevel composite rate equations in the steady-state limit are presented. The techniques discussed are generalization of those given in Sec. IV. Here allowance is made for more than one laser transition. Also, the general forms of the solutions will be discussed.

Practically speaking, only those equations containing laser-pumping terms need to be treated and solved as simultaneous equations, since their solutions can be directly substituted into the equation(s) for the unpumped level(s). As an example, consider the five-level model for sodium discussed in Sec. IV. Equations (77) can be solved in the following manner. (i) Solve the equations for N_1, N_2, N_4, and N_5 (N_3 has no laser term), while temporarily treating the $\mathcal{N}_i$ ($i=1,2,4,5$) as constants. (ii) Integrate the results over velocity to obtain four coupled equations for $\mathcal{N}_i$. (iii) Solve these equations simultaneously for $\mathcal{N}_1$, $\mathcal{N}_2$, $\mathcal{N}_4$, and $\mathcal{N}_5$. (iv) Substitute these solutions into the expressions found in step (i) for N_1, N_2, N_4, and N_5. (v) Solve the equation for N_3 in terms of $\mathcal{N}_3$, $\mathcal{N}_4$, and $\mathcal{N}_5$, and integrate over velocity to find $\mathcal{N}_3$. (vi) Finally, substitute the solution for $\mathcal{N}_3$ into the expression for N_3 found in step (v).

The solutions to the composite three-level model have the same general form as those derived in Sec. III. For models involving more than a single laser transition, such as those for sodium, the situation can be much more complicated. In these cases the solutions usually take the form of quotients of polynomials,[15] which often contain large numbers of terms.

For the velocity-selective case the general solution for a system with m ($l\rightarrow u$) laser transitions is given by

$$N_l=\frac{\sum_u[F_u^{(l)}(S_1\mathscr{L}_1,S_2\mathscr{L}_2,\ldots,S_m\mathscr{L}_m)]W_e\mathcal{N}_u+\sum_l[F_l(S_1\mathscr{L}_1,S_2\mathscr{L}_2,\ldots,S_m\mathscr{L}_m)]\left[W_g\mathcal{N}_l+\frac{N_l^{(0)}}{T}\right]}{F_\Delta(S_1\mathscr{L}_1,S_2\mathscr{L}_2,\ldots,S_m\mathscr{L}_m)},$$

$$N_u=\frac{\sum_u[F_u(S_1\mathscr{L}_1,S_2\mathscr{L}_2,\ldots,S_m\mathscr{L}_m)]W_e\mathcal{N}_u+\sum_l[F_l^{(u)}(S_1\mathscr{L}_1,S_2\mathscr{L}_2,\ldots,S_m\mathscr{L}_m)]\left[W_g\mathcal{N}_l+\frac{N_l^{(0)}}{T}\right]}{F_\Delta(S_1\mathscr{L}_1,S_2\mathscr{L}_2,\ldots,S_m\mathscr{L}_m)}, \tag{A1}$$

$$\frac{\mathcal{N}_{l(u)}}{N_{\rm tot}}=\frac{\sum_{l(u)}\mathscr{F}_{l(u)}(Z_1,Z_2,\ldots,Z_m)}{\mathscr{F}_\Delta(Z_1,Z_2,\ldots,Z_m)},$$

where the F's and $\mathscr{F}$'s are polynomials in $S\mathscr{L}$ and Z (defined below), respectively, $G(x)$ is given by Eq. (15), and $N_l^{(0)}=\mathcal{N}_l^{(0)}G(x)$. Note that $F_u^{(l)}\neq F_u$ and $F_l^{(u)}\neq F_l$. Now each ith $l\rightarrow u$ laser transition ($R_{ul}=R_{lu}$) generates both an $S\mathscr{L}$ and a Z factor, which are defined as

$$S_i=\frac{I}{I_S^{(i)}},$$
$$Z_i=\frac{I}{I_{\rm op}^{(i)}}, \tag{A2}$$

where $I_S^{(i)}$ and $I_{\rm op}^{(i)}$ are the usual saturation and optical-pumping intensities, respectively, and are given by

$$I_S^{(i)}=\left[\frac{\gamma_e}{\gamma_e+\frac{g_l}{g_u}\gamma_g-\Gamma_i}\right]\frac{\hbar\omega}{\bar\sigma_{iH}}\gamma_g,$$
$$I_{\rm op}^{(i)}=\left[\frac{\gamma_e}{\gamma_e+\frac{g_l}{g_u}\gamma_g-\Gamma_i}\right]\frac{\hbar\omega}{\bar\sigma_{iD}}\gamma_g\sqrt{1+S_i}, \tag{A3}$$

where

$$\gamma_e=\frac{1}{\tau}+\Gamma_e^v+\frac{1}{T},$$
$$\gamma_g=\Gamma_g^v+\frac{1}{T}, \tag{A4}$$
$$\Gamma_i=\Gamma_{ul}.$$

The average homogeneous $\bar\sigma_{iH}$ and Doppler $\bar\sigma_{iD}$-broadened absorption cross sections are defined as

$$\bar\sigma_{iH}=\frac{\sigma_{iH}^{\rm tot}}{g_l},$$
$$\bar\sigma_{iD}=\frac{\sigma_{iD}^{\rm tot}}{g_l}. \tag{A5}$$

For example, the $i=1\rightarrow4$ laser transition in the sodium five-level model (see Sec. IV) has g_l (level 1) $=3$, g_u (level 4) $=3$, $\sigma_{(14)H}^{\rm tot}=\pi\lambda\!\!\!^{-2}(\gamma_N/\gamma_H)$, so $\bar\sigma_{(14)H}=\frac{1}{3}\pi\lambda\!\!\!^{-2}(\gamma_N/\gamma_H)$, and so

$$I_S^{(14)}=\left[\frac{\gamma_e}{\gamma_e+\gamma_g-\Gamma_{41}}\right]\frac{\hbar\omega}{\bar\sigma_{(14)H}}\gamma_g,$$
$$I_{\rm op}^{(14)}=\left[\frac{\gamma_e}{\gamma_e+\gamma_g-\Gamma_{41}}\right]\frac{\hbar\omega}{\bar\sigma_{(14)D}}\gamma_g\sqrt{1+S_{14}}. \tag{A6}$$

As mentioned earlier, the polynomials can be quite complicated in that they can contain very many terms (e.g., those for the sodium five level model contain well in excess of one hundred terms[15]). Product terms, such as $(S_1\mathscr{L}_1)(S_2\mathscr{L}_2)$, Z_1Z_2, $(S_1\mathscr{L}_1)(S_2\mathscr{L}_2)(S_3\mathscr{L}_3)$, etc., are by far the most numerous [e.g., see Eqs. (72)]. The exact number and form of the products are determined by the number of pumped levels and laser transitions. Note that, terms of the form constant times $(S\mathscr{L})^n$ or Z^n $(n=2,3,\ldots)$ cancel and so do not appear in Eqs. (A1). When, instead of a single tunable laser field, there are j $(j=2,3,\ldots)$ separately tunable fields then $I\rightarrow I_j$; so that $S_i\rightarrow S_i^{(j)}$, $\mathscr{L}_i\rightarrow\mathscr{L}_i^{(j)}$, $Z_i\rightarrow Z_i^{(j)}$, with $S_i^{(j)}=I_j/I_S$, $Z_i^{(j)}=I_j/I_{\rm op}$, $\Delta_i\rightarrow\Delta_i^{(j)}$ $(=\Omega^j-\omega_i)$, etc. So, in addition to summations over u and 1 in Eqs. (A1), there are now sums over j, one for each independent laser field. So, for example,

$$\sum_u F_u(S_1\mathscr{L}_1,\ldots,S_m\mathscr{L}_m)\rightarrow\sum_u\sum_j F_u^{(j)}(S_1^{(j)}\mathscr{L}_1^{(j)},\ldots,S_m^{(j)}\mathscr{L}_m^{(j)}),\quad\text{etc.}$$

In cases where the ground- or excited-state (or both) hf splittings are less than the Doppler width, the relevant laser transitions can be pumped by a single field (see Sec. IV). Then the polynomials can be greatly simplified by neglecting all of the product terms. This follows from the fact that when one transition is resonant the others are off resonance by the hf splitting (since there is only one field) and are thus much smaller because the Lorentzian and Gaussian functions decrease fairly rapidly with frequency. Therefore, to a good approximation, the product terms can be dropped and the polynomials written as

$$F(S_1\mathscr{L}_1,\ldots,S_m\mathscr{L}_m)=\sum_{i=1}^{m}a_i(S_i\mathscr{L}_i)\,,\qquad \mathscr{F}(Z_1,\ldots,Z_m)=\sum_{i=1}^{m}\alpha_i Z_i\,, \tag{A7}$$

where a_i and α_i are various combinations of γ_e,γ_g and branching rates Γ_i. (There are similar expressions for F_Δ and $\mathscr{F}_\Delta$.) As an example, in the sodium five-level model $(m=4)$ terms containing $\mathscr{L}_{14}\mathscr{L}_{15}$, and $\mathscr{L}_{14}\mathscr{L}_{24}$ are negligible compared to those containing only $\mathscr{L}_{14}$, $\mathscr{L}_{15}$, or $\mathscr{L}_{24}$. The solutions are then given by

$$N_{l(u)}=\frac{\displaystyle\sum_{u(l)}\left[\sum_i a_i^{u(l)}(S_i\mathscr{L}_i)\right]W_e\mathscr{N}_u+\sum_{l(u)}\left[\sum_i b_i^{l(u)}(S_i\mathscr{L}_i)\right]\left[W_g\mathscr{N}_l+\frac{N_l^{(0)}}{T}\right]}{1+\displaystyle\sum_i C_i(S_i\mathscr{L}_i)}\,, \tag{A8}$$

where a_i and b_i, etc., are constants for a given buffer-gas pressure. For example, in the four-level system shown in Fig. 5(b) (for the moment neglecting degeneracy) N_1 is given by

$$N_1=\left\{\left[\frac{\Gamma_1}{\gamma_e\gamma_g}\right]\left[1+\left[\frac{\gamma_e}{\gamma_e+\gamma_g-\Gamma_2}\right]S_2\mathscr{L}_2\right]W_e\mathscr{N}_0+\left[\frac{1}{\gamma_g}\right]\left[1+\left[\frac{\gamma_e-\Gamma_2}{\gamma_e+\gamma_g-\Gamma_2}\right]S_2\mathscr{L}_2\right]\left[W_g\mathscr{N}_1+\frac{N_1^{(0)}}{T}\right]+\left[\frac{\Gamma_1/\gamma_g}{\gamma_e+\gamma_g-\Gamma_2}\right]S_2\mathscr{L}_2\left[W_g\mathscr{N}_2+\frac{N_2^{(0)}}{T}\right]\right\}\Big/(1+S_i\mathscr{L}_1+S_2\mathscr{L}_2)\,, \tag{A9}$$

where $l=1,2$, $u=0$, $i=2$ refers to the $2\rightarrow0$ $(0\rightarrow2)$ transition (Γ_2, S_2, and $\mathscr{L}_2$), and $i=1$ denotes the $1\rightarrow0$ $(0\rightarrow1)$ transition.

Even though the expressions for N_l and N_u are now much simpler, they remain difficult to integrate analytically over velocity to obtain $\mathscr{N}_l$ and $\mathscr{N}_u$. This is because their denominator is a sum of different Lorentzians (one for each laser transition). However, since their widths (γ_H) are usually much less than the hf splittings, the Lorentzian does not significantly overlap, and Eqs. (A8) can be further simplified by expanding them in terms of their resonant contributions. That is, for each ith $(l\rightarrow u)$ laser transition

$$N_{l(u)}=\sum_i\left[\frac{\text{Terms in }(S_i,\mathscr{L}_i,\mathscr{N}_i)}{1+S_i\mathscr{L}_i}\right]_{l(u)}\,, \tag{A10}$$

where the numerator contains sums over all relevant upper and lower levels (i.e., $\sum_l+\sum_u$). Note that the expression for N_l reduces $N_l=(1/\gamma_g)(W_g\mathscr{N}_l+\mathscr{N}_l^{(0)}/T)$, which is the background (i.e., $I=0$) population for level l.

Now when $N_u\cong0$ (fast radiative branching) Eqs. (A10) can be further simplified by dropping all excited-state terms. For instance, Eq. (A9) reduces to

$$\gamma_g N_1=\left[\frac{1}{1+S_i\mathscr{L}_i}\right]\left[W_g\mathscr{N}_1+\frac{N_1^{(0)}}{T}\right]+\left[\frac{\Gamma_1}{\gamma_e+\gamma_g-\Gamma_2}\right]\left[\frac{S_2\mathscr{L}_2}{1+S_2\mathscr{L}_2}\right]\times\left[W_g\mathscr{N}_2+\frac{N_2^{(0)}}{T}\right]. \tag{A11}$$

Mathematically speaking, the broadband case is much

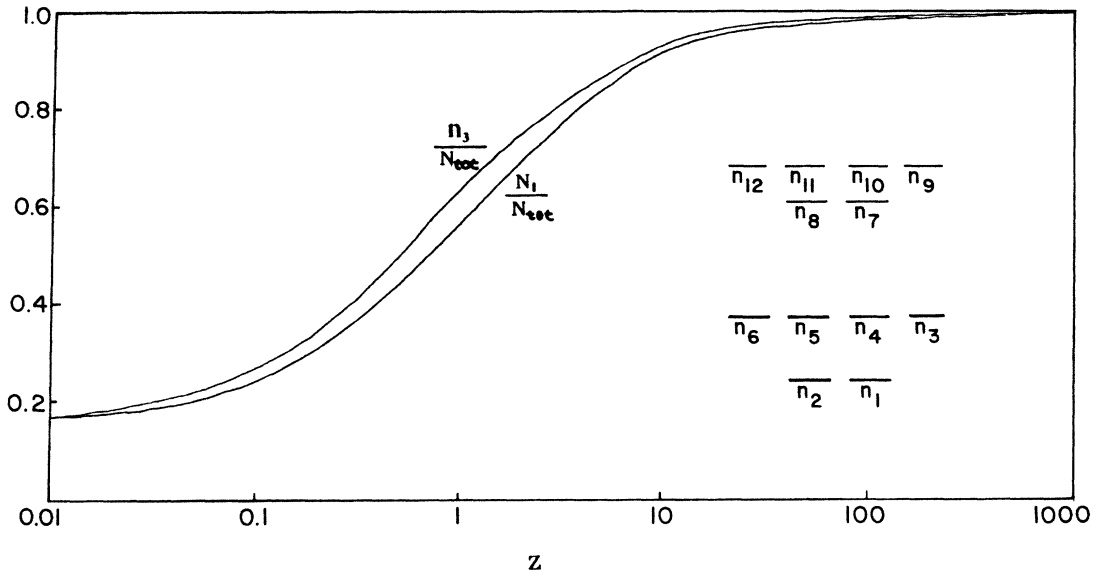

FIG. 7. 12-level system for ^{6}Li-$D1$ transition, and comparison between Eqs. (B1) and (B2).

simpler because no velocity integration is required. Then the $\mathcal{N}$'s are of the same form as Eq. (A1) [also see Eqs. (72)] but with

$$I_{\rm op}^{(lu)}=\left[\frac{\gamma_e}{\gamma_e+\frac{g_l}{g_u}\gamma_g-\Gamma_{ul}}\right]\frac{\hbar\omega}{\bar{\sigma}_{(lu)D}}\gamma_g\ , \tag{A12}$$

where

$$\gamma_e=\frac{1}{\tau}+\frac{1}{T}\ ,\qquad \gamma_g=\frac{1}{T}\ . \tag{A13}$$

When the ground-state hf splitting is much larger than the Doppler width more than one laser is required to achieve efficient optical pumping. In this case, the lasers are separately tunable and, in general, the product terms in Eqs. (A1) must be retained. Consequently, the approximation discussed above no longer applies and numerical methods must be used to evaluate the velocity integrals.

APPENDIX B: COMPARING COMPOSITE AND EXACT MODELS

To gain some idea of the accuracy of the composite models, a comparison between the ^{6}Li-$D1$ composite three-level model of Sec. IV and a full 12-level one was carried out in Ref. 15. Only the results for the broadband limit will be presented here.

In the three-level broadband limit, the population $\mathcal{N}_1$ of the unpumped $F=\frac{3}{2}$, $M_F=\frac{3}{2}$ sublevel can be written as

$$\frac{\mathcal{N}_1}{N_{\rm tot}}=\frac{27Z+5}{27Z+30}\ , \tag{B1}$$

where $Z=rT$, and

$$r=\frac{\sigma_D I}{\hbar\omega}\ ,$$

with

$$\sigma_D=\tfrac{4}{9}\pi\lambda\!\!\!^{-2}\frac{\gamma_H\sqrt{\pi}}{2ku}e^{-(\Delta/ku)^2}\ .$$

On the other hand, the solution for the complete 12-level (see Fig. 7) case is given by

$$\frac{\mathcal{N}_3}{N_{\rm tot}}=1-\frac{1}{6}\left[\frac{(4\,186\,100)Z^5+(4\,440\,400)Z^4+(7\,839\,200)Z^3+(373\,000)Z^2+(37\,152)Z+1458}{(1\,591\,812)Z^6+(3\,069\,180)Z^5+(2\,288\,489)Z^4+(855\,936)Z^3+(171\,450)Z^2+(17\,604)Z+729}\right.$$

$$\left.+\frac{(4950)Z^2+(1860)Z+762}{(5202)Z^3+(4799)Z^2+(1088)Z+81}+\frac{3}{3+17Z}\right]\ . \tag{B2}$$

Both of these results are plotted together in Fig. 7. The two curves asymptotically approach each other and the value 1 for large Z (i.e., for combinations of high intensities and buffer-gas pressures). Both converge to their zero-field equilibrium value $\frac{1}{6}$ for $Z=0$. The curves diverge for intermediate values of Z, with the largest separation occurring around saturation, indicating that the 12-level model saturates at somewhat lower intensities and pressures than the three-level one. As the figure shows, the results of the two approaches are fairly close, hence indicating that the three-level composite model is a reasonably good approximation to the much more complicated 12-level one.

[1]M. S. Feld, *Lasers in Nuclear Physics,* edited by C. E. Bemis, Jr. and H. K. Carter (Harwood Academic Press, Chur, 1982), p. 1, and other articles therein.

[2]L. W. Anderson, Nucl. Instrum. Methods **167**, 363 (1979).

[3]W. D. Cornelius, D. J. Taylor, R. L. York, and E. A. Hinds, Phys. Rev. Lett. **49**, 870 (1982).

[4]P. G. Pappas, R. A. Forber, W. W. Quivers, Jr., R. R. Dasari, and M. S. Feld, Phys. Rev. Lett. **47**, 236 (1981).

[5]Very recently laser optical pumping with VCC has produced a highly polarized ^{6}Li target for parity nonconservation studies of the reaction ^{6}Li$(\alpha,\gamma)^{10}$B, D. E. Murnick, private communication.

[6]M. Burns, P. G. Pappas, M. S. Feld, and D. E. Murnick, Nucl. Instrum. Methods **141**, 429 (1977).

[7]R. M. Kulsrud, H. P. Furth, E. J. Valeo, and M. Goldhaber, Phys. Rev. Lett. **49**, 1248 (1982).

[8]L. W. Anderson, Nucl. Instrum. Methods **158**, 57 (1979).

[9]A. C. Tam, J. Appl. Phys. **50**, 117 (1979).

[10]N. D. Bhaskar, N. Hou, M. Lesare, B. Suleman, and W. Happer, Phys. Rev. A **22**, 2710 (1980).

[11]W. W. Quivers, Jr. *et al.*, *Laser Spectroscopy V,* edited by A. R. W. McKeller, T. Oka, and B. P. Stoicheff (Springer-Verlag, Berlin, 1981), p. 186.

[12]C. H. Holbrow *et al.*, Phys. Rev. A **34**, 2477 (1986).

[13]See, for example, P. F. Liao, J. E. Bjorkolm, and P. R. Berman, Phys. Rev. A **21**, 1927 (1980); R. Vetter, C. Brechisnac, and P. R. Berman, Phys. Rev. A **17**, 1609 (1978); P. R. Berman, P. F. Liano, and J. E. Bjorkholm, Phys. Rev. A **20**, 2389 (1979).

[14]See, for example, M. Pinard, C. G. Aminoff, and F. Laloe, Phys. Rev. A **19**, 2366 (1979); R. Walkup, A. Spielfiedel, W. D. Phillips, and D. E. Pritchard, Phys. Rev. A **23**, 1869 (1981).

[15]W. W. Quivers, Jr., Ph.D. thesis, M.I.T., 1982 (unpublished).

[16]G. Shimkaveg *et al.*, Phys. Rev. Lett. **53**, 2230 (1984); *Spectroscopy VI* (in press).

[17]See, for example, W. Happer, Rev. Mod. Phys. **44**, 169 (1972).

[18]M. Borenstein and W. E. Lamb, Phys. Rev. A **5**, 1311 (1972).

[19]The theory, because it is based on rate equations, cannot describe such phenomena as coherent two-photon processes, which require the use of the density matrix. However, due to rapid excited-state radiative branching, the excited-state population, on average, is significant for usual intensities (less than a few W/cm^2), and so these processes can be neglected (see Refs. 15 and 20). Furthermore, coherent processes only affect the narrow resonance features and not the optical-pumping pedestals, which are pure rate-equation effects. Also along as $\Delta\nu_{g(e)}$ these effects will generally be small.

[20]M. S. Feld, M. M. Burns, T. U. Kuhl, P. G. Pappas, and D. E. Murnick, *Laser Spectroscopy IV,* edited by H. Walther and K. W. Rothe (Springer-Verlag, Berlin, 1979), p. 195.

[21]See, for example, P. R. Berman, *Advances in Atomic and Molecular Physics,* edited by D. R. Bates and B. Bederson (Academic, New York, 1977), Vol. 13, p. 57; P. R. Berman, Phys. Rep. **43**, 101 (1978).

[22]Actually Eq. (14) is the strong-collision limit of the Keilson-Storer kernel with zero "persistence of velocity" (e.g., see Ref. 13, 20, or 23).

[23]J. Keilson and J. E. Storer, Q. Appl. Math. **10**, 243 (1952).

[24]For example, see H. G. C. Werij, J. P. Woerdman, J. J. M. Beenakker, and I. Kuscer, Phys. Rev. Lett. **52**, 2237 (1984).

[25]This will always be the case for the broadband limit when $ku \gg \Delta\nu_e$. For the velocity-selective case the narrow resonances are only separated by $\Delta\nu_e$.

[26]Here there is only one narrow resonance feature for the velocity-selective case, and, of course, more for the broadband limit. This is effectively a three-level system in this instance.

[27]Due to the pumping scheme, and the fact that $\Delta\nu_{g(e)} \gg \gamma_H, ku$, there were no common levels, so that coherent two-photon processes were not present.